TASK QUARTERLY 6 No 3 (2002), 411–428

NUMERICAL ANALYSIS OF BEHAVIOUR OF REINFORCED CONCRETE ELEMENTS UNDER ECCENTRIC COMPRESSION

TOMASZ MAJEWSKI AND JACEK TEJCHMAN

Civil Engineering Department, Gdansk University of Technology,
Narutowicza 11/12, 80-952 Gdansk, Poland
{*tomimaj,tejchmk*}*@pg.gda.pl*

(Received 26 April 2002)

Abstract: Paper presents results of numerical modelling of behaviour of plane strain reinforced concrete elements under eccentric compression. In the analysis, a finite element method was used based on an elasto-plastic constitutive law by Drucker-Prager with hardening and softening for concrete and an elasto-plastic constitutive law by von Mises for reinforcement. The effects of boundary conditions at the element ends, eccentricity of the compressive load, element slenderness, area of the longitudinal and horizontal reinforcement on the load bearing capacity of elements were studied. The effect of the mesh refinement on the bearing capacity of elements was also analysed. A satisfactory agreement with model tests was achieved.

Keywords: eccentric compression, concrete, finite element method, reinforced concrete, reinforcement

1. Introduction

Reinforced concrete columns and walls supporting slabs and beams are frequently subject to eccentric compression. The calculation of the bearing capacity of such elements is, however, difficult since it depends upon many different factors such as: element slenderness, load eccentricity, boundary conditions at the ends, area and shape of the cross-section of concrete, area and spacing of the vertical and horizontal reinforcement, reinforcement ratio, compressive strength of concrete, compressive and tensile strength of reinforcement, type and character of load (short or long-term, monotonic or cycling), concrete shrinkage and concrete creep. To calculate the optimal reinforcement area and thus to decrease building costs, a theoretical prediction of the influence of these factors on stresses in the entire element is needed. To obtain this information, a finite element method can be used [1–4].

The intention of the paper is to numerically analyse the behaviour of plane strain reinforced concrete elements (walls) subject to eccentric compression. The analysis was carried out with a conventional finite element method. The material and geometric non-linearities were taken into account. To describe plain concrete for monotonic loading without confining pressures, an elastic-plastic smeared crack constitutive law by Drucker-Prager with isotropic hardening and softening was used.

In turn, the behaviour of reinforcement was modelled by an elasto-plastic constitutive law by von Mises with isotropic hardening. During calculations, both a full interaction and a full slip between concrete and reinforcement was considered. The effect of load eccentricity, boundary conditions at the element ends, element slenderness, area of the longitudinal and horizontal reinforcement on the bearing capacity of elements was studied. The effect of the mesh refinement was analysed as well. Due to the lack of comprehensive experiments carried out with reinforced concrete walls, the numerical calculations were compared with results of laboratory tests performed on columns by Kim and Yang [5].

The bearing capacity of reinforced concrete columns was experimentally studied by many researchers. The effect of the load eccentricity was investigated by Makovi [6], Gruber and Menn [7], Kiedroń [8], Billinger and Symons [9], Lloyd and Rangan [10]. Billinger and Symons [9], and Kim and Yang [5] studied the effect of the column slenderness. Szuchnicki [11] analysed the influence of the cross-section. In turn, the effect of creep was investigated by Kordina *et al.* [12], the effect of lateral prestressing by Gardner *et al.* [13], the effect of the vertical reinforcement by Kim and Yang [5], Lloyd and Rangan [9], and the effect the horizontal reinforcement by Oleszkiewicz *et al.* [14] and Korzeniowski [15, 16]. In turn, the influence of the concrete strength was shown in tests by Kim and Yang [5], Kiedroń [7], Billinger and Symons [8], and Lloyd and Rangan [9]. The results of experiments have evidently shown that bearing capacity of columns decreases with increasing load eccentricity, slenderness, ratio of the end fixing and creep. The increase of concrete strength influences significantly the bearing capacity for small eccentricities. The lateral prestressing and horizontal reinforcement increase the bearing capacity of cylindrical elements.

There exist several theoretical models to calculate the bearing capacity of elements under eccentric compression. A satisfactory agreement between experimental and theoretical results was achieved with a numerical uniaxial model proposed by Korzeniowski [15, 17], Fragomeni and Mendis [18], and Mendis [19].

The paper is organised as follows. At the beginning, basic assumptions incorporated in the formulation of a constitutive model for concrete and reinforcement are outlined. Later, the details of finite element implementation are given. Next, the numerical results on reinforced concrete element subject to eccentric load are described to demonstrate the validity of the numerical model. The results are compared with model tests. Finally, general conclusions from the theoretical research are provided.

2. Constitutive model for concrete

The behaviour of concrete has been the object of intensive research over the last few decades. Despite of many significant contributions, the description of the mechanical response of concrete still poses a formidable challenge. It is because concrete is a discrete, strongly heterogeneous material and its behaviour is very complex due to localised modes during the damage (micro- and macro-cracks, shear zones). The most important properties of concrete are:

- compressive strength is several times higher than tensile one,
- elastic behaviour takes place up to one third of the compressive strength during uniaxial compression and up to two third of the tensile strength by uniaxial extension,
- during biaxial compression, compressive strength is about 20–30% higher than during uniaxial one,
- failure surface is close to parabolic in a principle stress space,
- shape of the failure surface in deviatoric planes changes from a curvilinear triangle for low hydrostatic pressures to nearly circular at high pressures,
- progressive transition from compaction to dilatancy is observed during compression,
- non-associated flow rule prevails,
- ductile (stable) damage occurs at high pressures and brittle (unstable) damage at low pressures,
- shear strength is different in a triaxial compression and extension test,
- elastic modulus depends on pressure,
- material is anisotropic,
- creep and shrinkage are of importance,
- scale effects in model tests due to localisation of deformations (cracks, shear zones) exist.

Continuum models describing the mechanical behaviour of concrete were formulated within non-linear elasticity [20–23], rate-independent plasticity [24–27], endochronic theory [28, 29], plastic-fracturing theory [30, 31] and lattice models [32]. Elasto-plastic models found, however, the widest application in solving of practical engineering problems. The simplest ones use criteria following Rankine, Coulomb-Mohr and Drucker-Prager with or without closing caps in the tensile and compression region [1, 33, 34]. Others to realistically describe the triaxial strength of concrete apply a non-linear Drucker-Prager criterium [35], parabolic Leon criterium [36], extended Leon criterium [37] and own formulations [2, 24, 26, 27, 38–40].

To model the behaviour of plain concrete elements under eccentric loading, in the first step, a linear non-associated Drucker-Prager constitutive law for concrete with isotropic hardening and softening was used which combines the cohesive strength of the cement paste with the frictional adhesion of aggregate interaction. The failure surface was closed in the tensile and compressive regime by a linear limit cap surface. Therein, a constant elastic modulus was used. The constitutive law can be summarised as follows:

$$\dot{\varepsilon}_{ij} = \dot{\varepsilon}^e_{ij} + \dot{\varepsilon}^p_{ij}, \tag{1}$$

$$\dot{\varepsilon}^p_{ij} = \lambda \frac{\partial g}{\partial \sigma_{ij}}, \tag{2}$$

$$\tau = (0.5 s_{ij} s_{ij})^{1/2}, \tag{3}$$

$$f = \tau + \mu(\kappa^p) p - c, \tag{4}$$

$$g = \tau + \alpha(\kappa^p) p, \tag{5}$$

wherein τ is the second invariant of the deviatoric stress tensor, s_{ij} – non-symmetric deviatoric stress tensor ($s_{ij} = \sigma_{ij} - p\delta_{ij}$), p – mean stress, σ_{ij} – stress tensor, f – yield

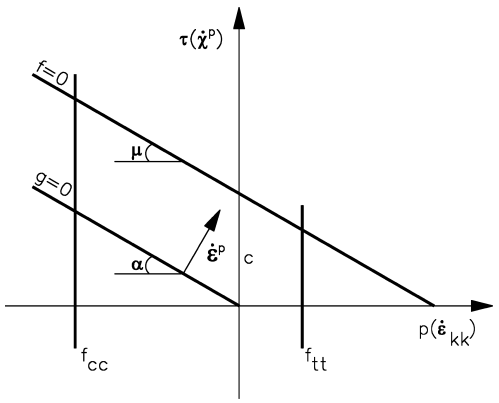

Figure 1. Yield and flow potential curves in the τ, p-plane

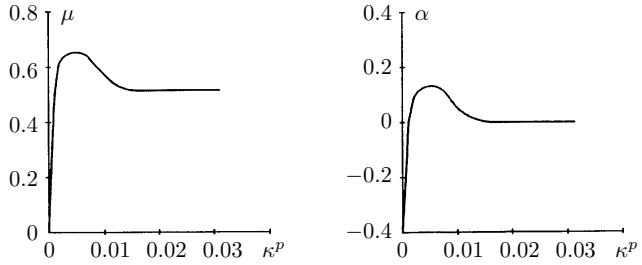

Figure 2. Measures of frictional strength $\mu = \sin\phi$ and volume change $\alpha = \sin\beta$ (ϕ – internal friction angle, β – dilatancy angle, κ^p – second invariant of the deviatoric deformation tensor)

function, g – potential function, μ – measure of the frictional strength, α – measure of the volume change, c – cohesive strength, κ^p – second invariant of the deviatoric deformation tensor, ε_{ij} – deformation tensor, $\dot{\varepsilon}_{ij}$ – rate of deformation tensor, λ – proportionality factor. The superimposed indexes e and p designate the elastic and the plastic deformation, respectively. In the τ, p-plane, the equations $f = 0$ and $g = 0$ describe a yield and a flow potential curve (Figure 1). The factors μ in Equation (4) and α in Equation (5) are related (similarly as for granular materials [41]) to the angle of internal friction ϕ ($\mu = \sin\phi$) and the angle of dilatancy β ($\alpha = \sin\beta$). They can be identified with the help of uniaxial compression test. Figure 2 shows the evolution of the assumed measures μ and α versus κ^p. At the beginning of deformation, the material behaves contractant and becomes dilatant if $\phi > \phi_{cr}$ (index cr stands for a critical (residual) value). To obtain realistic values of the tensile and compressive strength, the failure surface was closed at the tensile and compressive side by linear caps described by (Figure 1):

$$p = -f_{cc}, \qquad p = f_{tt}, \tag{6}$$

where f_{cc} and f_{tt} are the biaxial compressive and biaxial tensile strength, respectively.

The constitutive law includes two functions to be estimated $\mu = f(\kappa^p)$ and $\alpha = f(\kappa^p)$, and 5 material parameters: E (elastic modulus), ν (Poisson's ratio), c, f_{cc} and f_{tt}.

When using constitutive models with material softening, the calculated FE-results show a pathological dependency on the mesh size [41–43]. It is because the

governing equations of motion change their type and the boundary value problem becomes, thus, mathematically ill-posed [44]. To avoid this deficiency, enriched approaches must be used which take into account a material (characteristic) length, such as: Cosserat [41, 44, 45], non-local [46, 47], higher order deformation gradient [44, 48] and viscous models [48, 49]. By taking into account a material length, scale effects can be captured [41–49]. The results presented in this paper do not depend strongly on the mesh refinement since the FE-studies were performed for a force-controlled case. Thus, only small softening region of concrete was taken into account.

3. Constitutive model for reinforcement

To simulate the behaviour of reinforcement, an associated elasto-plastic constitutive law by von Mises with isotropic hardening was assumed. In this case, the yield and potential functions are:

$$f = g = \tau - \sigma_y(\kappa^p). \tag{7}$$

The equivalent yield strength function σ_y is shown in Figure 3 (f_{yd} – yield stress).

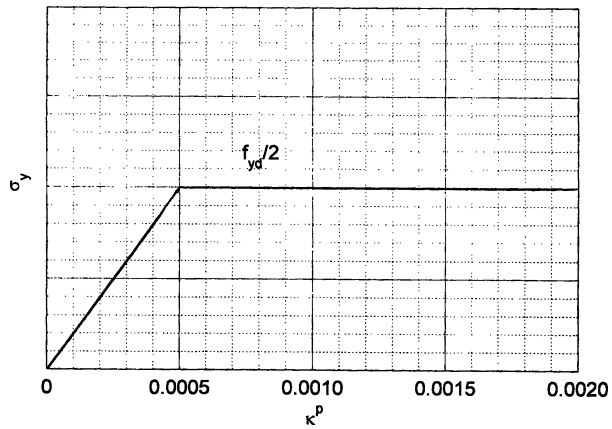

Figure 3. Equivalent yield strength function σ_γ versus second invariant of the deviatoric deformation tensor κ^p assumed for reinforcement ($f_{\gamma d}$ – yield stress)

4. Initial FE-studies

4.1. Finite element data

During initial FE-calculations, the effects of the following parameters on the element behaviour were carefully investigated:

- eccentricity,
- boundary conditions at the top,
- slenderness,
- area of the vertical reinforcement,
- horizontal reinforcement and
- mesh discretisation.

The height of the wall was $h = 0.80\text{m}$, width $b = 0.04\text{m}$ $(h/b = 20)$ and length $l = 1.0\text{m}$ (plane strain) To investigate the effect of the mesh on the results,

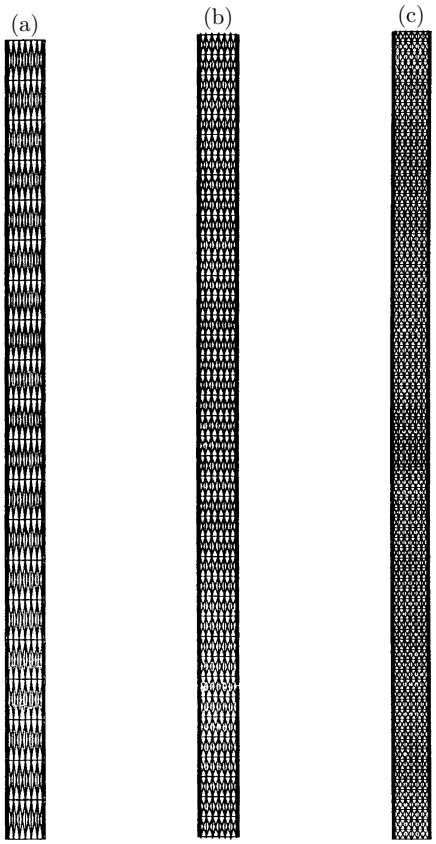

Figure 4. Meshes used for FE-calculations: (a) loose, (b) dense, (c) fine

three different discretisations have been used, namely a 10×20-mesh, a 10×40-mesh and 10×80-mesh, where each quadrilateral is composed of four triangular elements (Figure 4). Using such elements, the effect of volumetric locking can be avoided [50]. Linear shape functions for displacements were applied. The calculations were carried out mainly with a fine mesh (Figure 4c). In this case, the height of all elements was 10mm and the width of elements along the cross-section was 2, 1, 5, 4×6, 5, 1 and 2mm. In the quadrilateral element columns located 2mm from both sides, the vertical symmetric steel bars with a width of 1mm were assumed. Thus, the reinforcement area was $As_1 = As_2 = 1000\,\mathrm{mm}^2$ and the reinforcement ratio $\rho = (As_1 + As_2)/(dl) = 2000/[(40 - 2.5) \times 1000] = 5.33\%$ (As_1 – reinforcement area in the less compressed zone or tensile zone, As_2 – reinforcement area in the more compressed zone, $d = 37.5\,\mathrm{mm}$ – effective width).

Quasi-static deformation was initiated through a monotonically increasing vertical load prescribed to the element top. To induce an eccentricity, vertical load on the top was applied. The load increment ΔP in each load step n was assumed to be $\Delta P = 1\,\mathrm{kN}$. The calculations were also performed with smaller steps (without the effect on results). The vertical force at which the loss of the calculation convergency (due to concrete softening) was assumed as the bearing capacity of the element. During this analysis, a smooth bottom was always fixed: the vertical displacement

of the bottom nodes was $u_2 = 0$ and the horizontal displacement of two sides nodes along the bottom was $u_1 = 0$. The smooth top was fixed (the horizontal displacement of two side nodes was $u_1 = 0$), free or had a hinge (the horizontal displacement of the mid-point $u_1 = 0$). Boundary conditions along the vertical sides were traction-free. A full interaction between the concrete and reinforcement was assumed.

As the initial stress state, the vertical normal stress $\sigma_{22} = \gamma_c x_2$ was assumed ($\gamma_c = 25\text{kN/m}^3$ denotes the volume weight of the concrete, x_2 is the vertical co-ordinate measured from the specimen top).

To take into account geometric non-linearities, the calculations were carried out with large deformations. In this case, an Updated Lagrangian formulation [51] was applied. The changes of the element configuration and the element volume were considered.

To satisfy the consistency condition $f = 0$, the trial stress method (linearised expansion of the yield condition about the trial stress point) using an elastic predictor and a plastic corrector with radial return mapping algorithm was applied [52].

For the solution of the non-linear equation of motion governing the response of a system of finite elements, a modified Newton-Raphson scheme with line search was used [51]. The calculations were performed using a symmetric elastic global stiffness matrix. The iteration steps were performed using convergence criteria based on translations (found by means of preliminary FE-calculations).

4.2. Numerical results

The following data were assumed for concrete during FE-calculations: $E = 20\,000\text{MPa}$, $\nu = 0.2$, $\phi_p = 40^\circ$, $\phi_{cr} = 30^\circ$, $\beta_p = 10^\circ$, $\beta_{cr} = 0^\circ$, $(\kappa^p)_p = 0.5\%$, $c = 3.9\text{MPa}$, $f_{tt} = 1.5\text{MPa}$ (p – peak value, cr – residual value), Figure 1. In the calculations, a linear cap in the compressive regime was neglected. The numerical calculations for reinforcement were performed with $E = 210\,000\text{MPa}$, $\nu = 0.3$ and $f_{\gamma d} = 200\text{MPa}$.

First, a plane strain FE-analysis for uniaxial compression and extension with a concrete specimen, and for uniaxial extension with a steel bar was carried out. Figure 5 presents the results for a concrete specimen with a height of $h = 80\text{mm}$, width of $b = 4\text{mm}$ and length $l = 1.0\text{m}$. Both top and bottom were assumed to be very smooth. In this study, constant vertical displacements were prescribed to the top boundary. The calculated uniaxial compressive strength, $f_c = P/(bl)$, is equal to $f_c = 22\text{MPa}$ for the vertical strain of the top $\bar{\varepsilon}_{22} = 0.2\%$ (Figure 4a), P is the resultant vertical force on the top. The residual strength is 16kPa. It is a fictitious value because the damage of concrete takes place after the peak in a softening regime before a residual strength is obtained. In turn, the uniaxial tensile strength is $f_t = 3\text{MPa}$ for the vertical strain of the top $\bar{\varepsilon}_{22} = 0.02\%$ (Figure 4b). With these calculated values of f_c and f_t, the cohesive strength assumed, $c = 3.9\text{MPa}$, is approximately equal to the shear strength following the Mohr's assumption [53]:

$$\tau = 0.5\sqrt{f_c f_t} = 0.5\sqrt{22 \cdot 3} = 4.0\text{MPa} \tag{8}$$

Figure 6 presents the calculated mean vertical force on the top of a steel bar with a height of $h = 80\text{mm}$ and a width of $b = 4\text{mm}$ for a very smooth top and bottom versus the vertical strain of the top. The uniaxial tensile yield strength, $f_\gamma = f_{\gamma d} = 200\text{MPa}$, is obtained for the vertical strain of the top $\bar{\varepsilon}_{22} = f_{yd}/E = 0.095\%$.

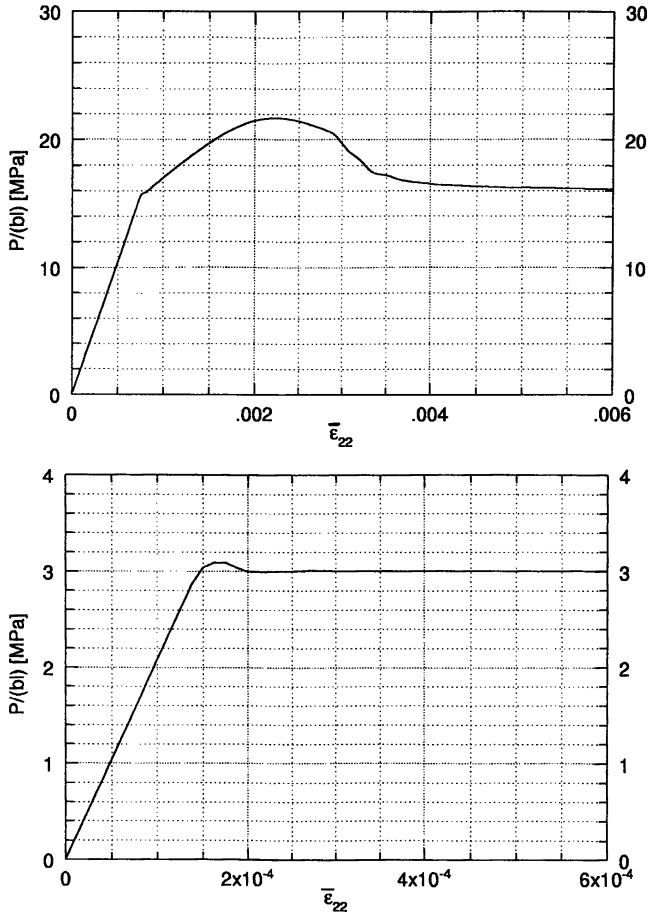

Figure 5. Calculated stress-strain curve during uniaxial compression and tension for the concrete specimen (P – vertical force on the top, $b = 0.04$m – specimen width, $l = 1$m – specimen length, $\bar{\varepsilon}_{22}$ – mean vertical strain)

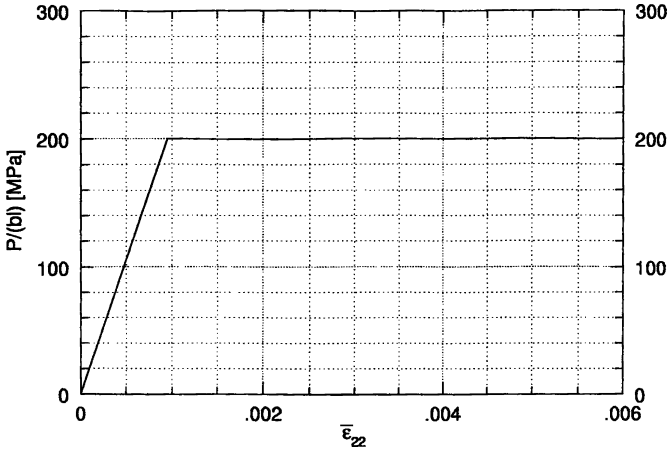

Figure 6. Calculated stress-strain curve during uniaxial tension for the steel bar (P – vertical force on the top, $b = 4$mm – specimen width, $l = 1$m – specimen length, $\bar{\varepsilon}_{22}$ – mean vertical strain)

Figures 7–15 demonstrate numerical results of the finite element simulation for reinforced concrete walls. The vertical stresses shown were calculated as mean values from four triangles creating one quadrilateral. The displacements of the mesh were magnified by the factor 20.

Figure 7 shows the FE-results for a centrally loaded wall (eccentricity $e = 0$) with a fixed both top and bottom. Presented is the evolution of vertical normal stresses σ_{22} in the concrete and reinforcement along the cross-section at the height of $H = h$, $H = 0.75h$ and $H = 0.5h$ (measured from the bottom) versus the loading

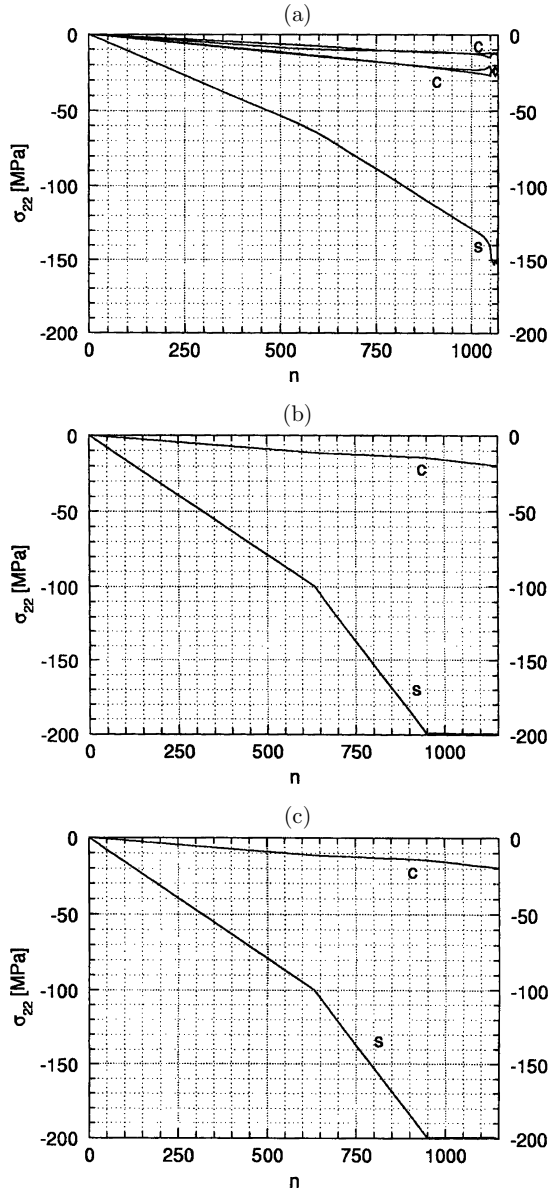

Figure 7. Vertical normal stresses versus load step n at (a) $H = h$, (b) $H = 0.75h$, and (c) $H = 0.5h$ from FE-calculations ($e/b = 0$, fixed-fixed end conditions, s – steel, c – concrete)

step n being equivalent to the vertical force on the top P. The normalised bearing capacity of the wall $N = P/(\gamma_c b^2 l)$ is equal to 26 500 and is by 15% smaller than this resulting from the multiplication of the uniaxial compressive strength of concrete $f_c = 22\text{MPa}$ (Figure 5) with the concrete area $A_c = 34\,000\text{mm}^2$, and the yield stress of reinforcement $f_{\gamma d} = 200\text{MPa}$ (Figure 6) with the reinforcement area $A_s = 2000\text{mm}^2$. The vertical displacement of the top changes from $u_2 = 3\text{mm}$ (edges) to $u_2 = 4\text{mm}$ (mid-point) for $n = 1100$. The vertical normal stresses reach in the concrete 20MPa ($H = 0.75h$ and $H = 0.5h$), and 12–25MPa ($H = h$). In turn, the vertical normal stresses σ_{22} in the reinforcement in a residual state are equal to $f_{\gamma d} = 200\text{MPa}$ in the entire wall except of the top region ($\sigma_{22} = 150\text{MPa}$). They show a small kick at the moment when concrete starts to behave plastically.

Figures 8–9 show the results for two eccentricities: $e/b = 0.2$ and $e/b = 0.3$ in the case of fixed-fixed boundary conditions. The normalised bearing capacity of the wall decreases strongly with increasing e/b: $N = 26\,500$ ($e/b = 0$), $N = 20\,000$ ($e/b = 0.2$) and $N = 16\,900$ ($e/b = 0.3$). The vertical normal stresses in the reinforcement in the less compressed zone are significantly smaller than $f_{\gamma d} = 200\text{MPa}$. They are fully developed in the more compressed zone at $H = 0.75h$ and $H = 0.5h$ ($e/b = 0.2$) and at $H = h$ and $H = 0.75h$ ($e/b = 0.3$). The vertical displacement of the top changes from 0.40mm to 0.84mm ($n = 700$, $e/b = 0.2$) and from 0.27mm to 0.78mm ($n = 600$, $e/b = 0.3$). The maximum horizontal displacement is equal to 1.25mm ($n = 700$, $e/b = 0.2$) and 1.35mm ($n = 600$, $e/b = 0.3$).

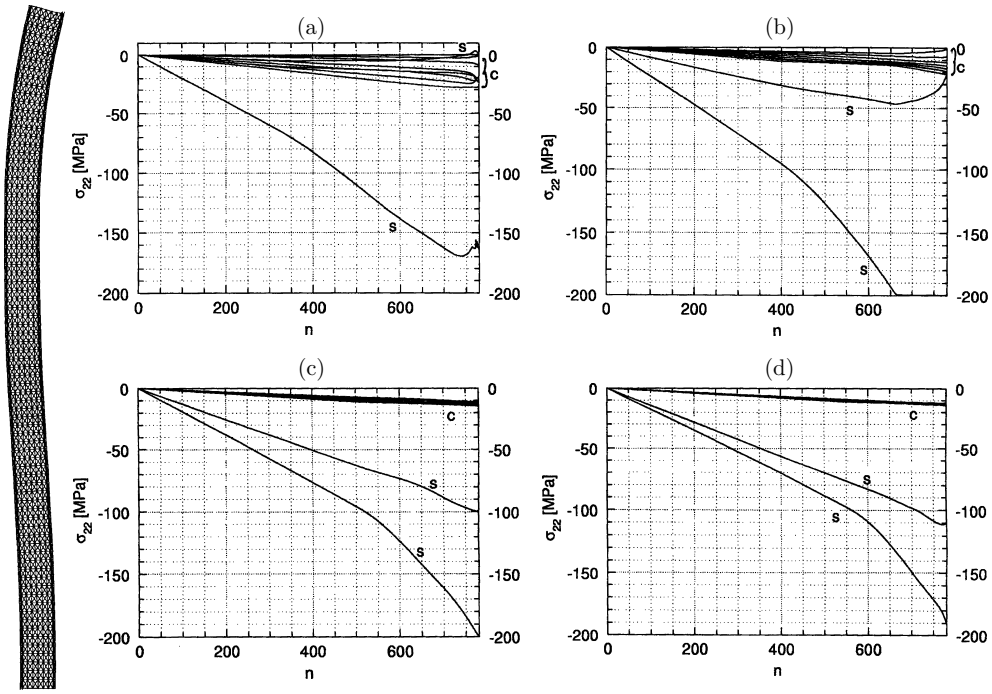

Figure 8. FE-calculations: deformed mesh ($n = 600$) and vertical normal stresses versus load step n at (a) $H = h$, (b) $H = 0.75h$, (c) $H = 0.5h$, and (d) $H = 0.25h$ for the case of $e/b = 0.2$ and fixed-fixed end conditions (s – steel, c – concrete)

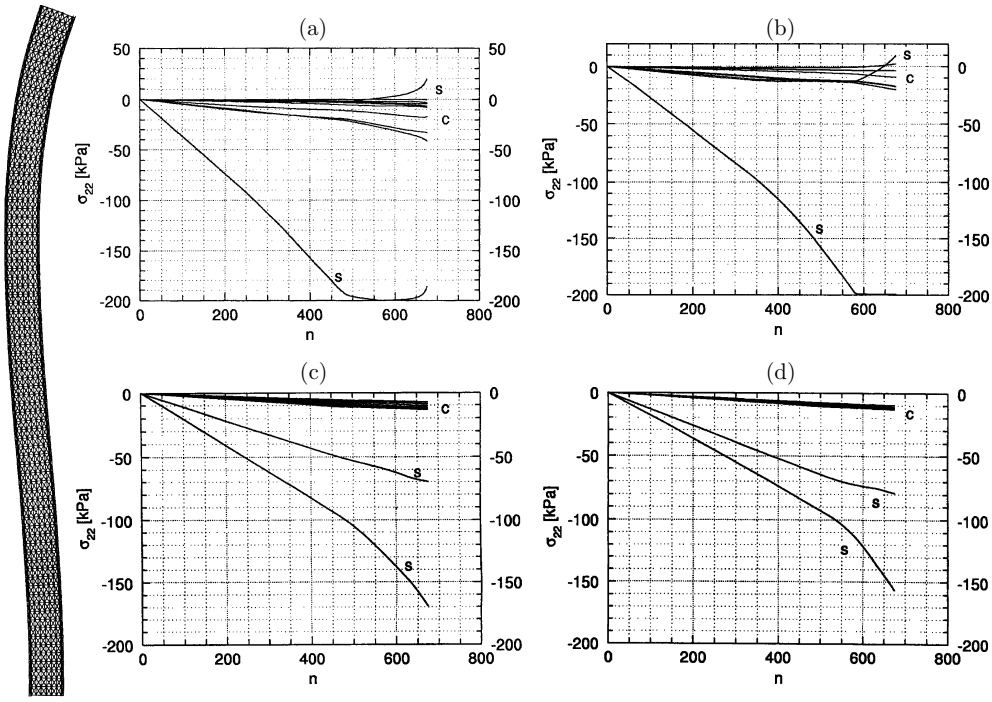

Figure 9. FE-calculations: deformed mesh ($n = 600$) and vertical normal stresses versus load step n at (a) $H = h$, (b) $H = 0.75h$, (c) $H = 0.5h$ and (d) $H = 0.25h$ for the case of $e/b = 0.3$ and fixed-fixed end conditions (s – steel, c – concrete)

The effect of the boundary condition at the top with $e/b = 0.3$ is presented in Figures 10–11. The normalised bearing capacity decreases significantly with increasing degrees of freedom. It is equal to $N = 16\,900$ (fixed-fixed end conditions), $N = 12\,125$ (fixed-hinge end conditions) and $N = 8000$ (fixed-free end conditions). For the case of fixed-free end conditions, the vertical displacement of the top changes from 0.15mm to 0.8mm, and the maximum horizontal displacement is 10.3mm ($n = 300$). In this case, the vertical normal stresses in the reinforcement and concrete (less compressed zone) reach a tensile region (except of the top region), Figure 11.

The decrease of the slenderness ratio h/b from 20 to 5 increases the normalised bearing capacity by about 20% ($e/b = 0.3$, fixed-fixed end conditions), Figure 12.

The decrease of the reinforcement area in the entire wall by the factor 5 ($As_1 = As_2 = 200\text{mm}^2$, $\rho = 1.07\%$, $\rho_1 = \rho_2 = 0.53\%$) decreases the normalised bearing capacity by 30% (Figure 13).

The calculations were carried out also with a smaller longitudinal reinforcement in the less compressed zone ($e/b = 0.3$, fixed-fixed end conditions). One assumed $As_1 = 1000\text{mm}^2$ and $As_2 = 200\text{mm}^2$. In this case, the bearing capacity of the wall was smaller by only 5%.

The results of the normalised bearing capacity of walls $N = P/(\gamma_c b^2 l)$ are summarised in Tab.1 for different e/b, h/b, ρ_1, ρ_2 and conditions at the top.

To investigate the effect of the horizontal reinforcement on the bearing capacity, some horizontal stir-ups along the wall height were added to vertical bars. One

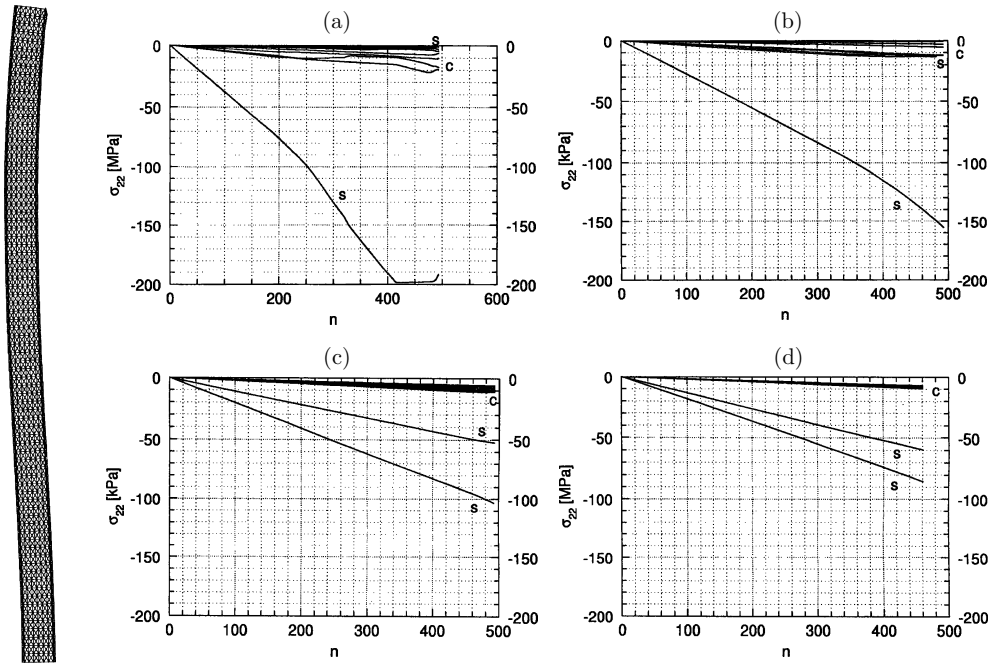

Figure 10. FE-calculations: deformed mesh ($n=400$) and vertical normal stresses versus load step n at (a) $H=h$, (b) $H=0.75h$, (c) $H=0.5h$, and (d) $H=0.25h$ for the case of $e/b=0.3$ and fixed-hinge end conditions (s – steel, c – concrete)

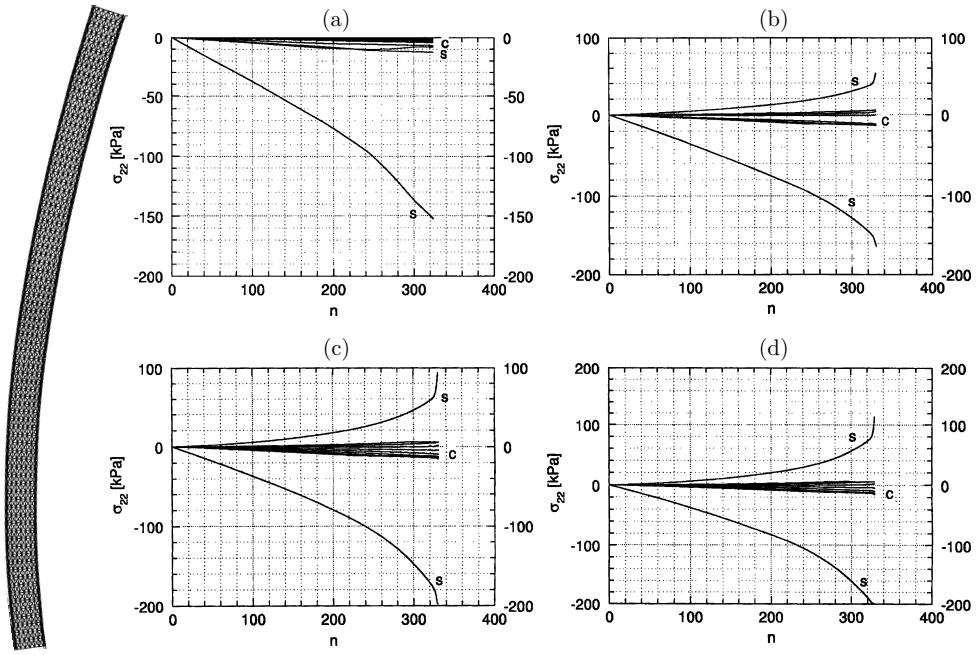

Figure 11. FE-calculations: deformed mesh ($n=600$) and vertical normal stresses versus load step n at (a) $H=h$, (b) $H=0.75h$, (c) $H=0.5h$, and (d) $H=0.25h$ for the case of $e/b=0.3$ and fixed-free end conditions (s – steel, c – concrete)

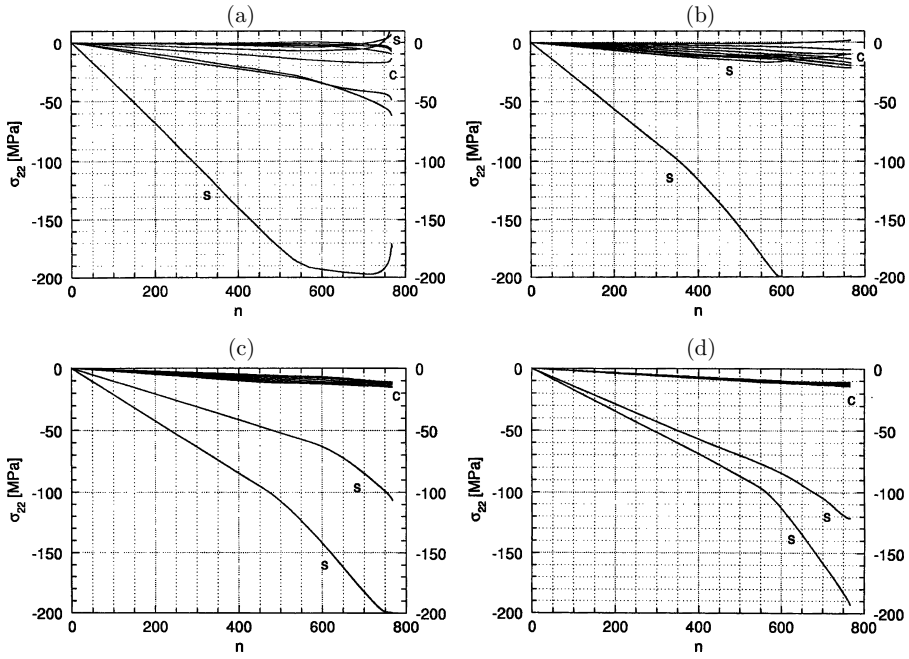

Figure 12. FE-calculations: vertical normal stresses versus load step n at (a) $H=h$, (b) $H=0.75h$, (c) $H=0.5h$, and (d) $H=0.25h$ for the case of $e/b=0.3$, $h/b=5$ and fixed-fixed end conditions (s – steel, c – concrete)

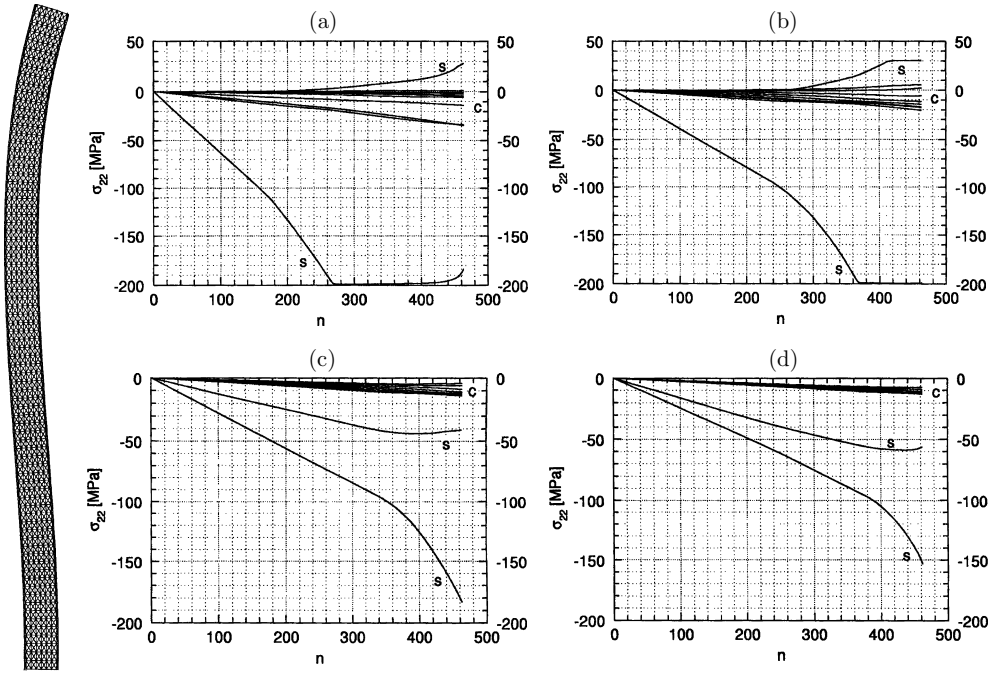

Figure 13. FE-calculations: deformed mesh ($n=400$) and vertical normal stresses versus load step n at (a) $H=h$, (b) $H=0.75h$, (c) $H=0.5h$, and (d) $H=0.25h$ for the case of $e/b=0.3$, $\rho_1=\rho_2=0.53\%$ and fixed-fixed end conditions (s – steel, c – concrete)

Table 1. Normalised bearing capacity of walls N

h/b	e/b	ρ_1 [%]	ρ_2 [%]	End conditions	$N = P/(\gamma_c b^2 l)$
20	0	2.67	2.67	fixed-fixed	26500
20	0.2	2.67	2.67	fixed-fixed	20000
20	0.3	2.67	2.67	fixed-fixed	16900
20	0.2	2.67	2.67	fixed-hinge	17075
20	0.3	2.67	2.67	fixed-hinge	12125
20	0.3	2.67	2.67	fixed-free	8000
5	0.3	2.67	2.67	fixed-fixed	20000
20	0.3	0.53	2.67	fixed-fixed	16250
20	0.3	0.53	0.53	fixed-fixed	11750

assumed 7 horizontal stir-ups with a thickness of 0.2mm or 1mm at the spacing of $s = 10$cm ($s/b = 2.5$). No increase of the bearing capacity was obtained.

The calculations with different meshes of Figure 4 showed that the maximum vertical force on the top with a fine mesh (Figure 4c) was in average by 5% smaller than in the case of a medium dense mesh (Figure 4b), and by 15% smaller than in the case of a coarse mesh (Figure 4c). Thus, one can assume that the calculated results with a mesh of Figure 4c would change only insignificantly when using a finer mesh.

5. Comparison with experiments

5.1. Model tests

In the experiments on 30 rectangular columns performed by Kim and Yang [5], the following parameters were varied: column slenderness ($h/b = 3$, 18, 30), longitudinal steel ratios ($\rho_1 = \rho_2 = 0.99$, 1.98%), compressive concrete strength ($f_c = 25.5$, 63.5, 86.2MPa). The cross-section of columns was $0.08 \times 0.08\,\mathrm{m}^2$, the height 0.24–2.4m and the eccentricity $e/b = 0.3$. The thickness of the concrete cover measured from the bar centre to the concrete surface was 15mm. The boundary conditions at the column ends were both hinged. The rate of loading was controlled by a constant rate of the vertical displacement. The vertical force on the top, lateral deflection and strains of deformed bar at the mid-height of columns were measured.

The experiments showed that columns with $h/b = 3$ failed at their mid-height by increased compressive strain, and columns with $h/b = 18$ and $h/b = 30$ by increased tensile strain. The maximum lateral deflection at the ultimate load was 0.4mm ($h/b = 3$), 15–16mm ($h/b = 18$) and 30–33mm ($h/b = 30$) with $\rho_1 = \rho_2 = 0.99\%$ and $f_c = 25.5$MPa, and 0.43mm ($h/b = 3$), 18–20mm ($h/b = 18$) and 26–27mm ($h/b = 30$) with $\rho_1 = \rho_2 = 0.99\%$ and $f_c = 63.5$MPa. The experiments revealed that the ultimate load for a short high-strength concrete column was significantly enhanced (but not for a slender column). The possibility of stability failure for a slender column was increased with an increase of concrete strength. The increment of the ultimate load due to an increase in longitudinal reinforcement for the short column was less than for a slender one, and the heavier reinforcement for a slender column led to a more stable column.

5.2. Numerical simulations

The numerical calculations were performed with a short and slender column from model tests of Section 5.1 ($b = 0.08$m, $e/b = 0.3$, $\rho_1 = \rho_2 = 0.99\%$, $fc = 25.5$MPa,

$f_{yd} = 387\text{MPa}$). In the first case (short column), the height was $h = 0.24\text{m}$ ($h/b = 3$). In the second case (slender column), the height was $h = 2.4\text{m}$ ($h/b = 30$). The 12×42-mesh consisted of 2016 triangular elements.

The following data were assumed for concrete: $E = 23\,665\text{MPa}$, $\nu = 0.2$, $\phi_p = 40^\circ$, $\phi_{cr} = 20^\circ$, $\beta_p = 10^\circ$, $\beta_{cr} = 0^\circ$, $(\kappa^p)_p = 0.3\%$, $c = 4.568\text{MPa}$, $f_{cc} = f_c = 25.5\text{MPa}$ $f_{tt} = f_t = 1.5\text{MPa}$ (Figure 1), and for reinforcement: $E = 210\,000\text{MPa}$, $\nu = 0.3$ and $f_{\gamma d} = 387\text{MPa}$.

The boundary conditions at the ends were both hinged. The top and the bottom were smooth. One node in the middle of the bottom and the top was fixed ($u_1 = 0$, $u_2 = 0$). A full slip between concrete and vertical reinforcement was assumed (horizontal displacements of nodes at the interface concrete-reinforcement were the same).

Figures 14–16 present the calculated results: deformed mesh and the evolution of vertical normal stresses σ_{22} in concrete and reinforcement along the cross-section at the height of $H = h$, $H = 0.75h$ and $H = 0.5h$ (measured from the bottom) versus the loading step n being equivalent to the vertical force P, and the axial force-lateral deflection diagrams. To compare the calculated ultimate load for walls with the experimental ones for columns, the calculated maximum vertical load on the wall top was multiplied with the factor 0.08 corresponding to the size of the cross-section of columns perpendicular to the loading plane.

In the case of a short column, the vertical normal stresses in the reinforcement are in the tensile zone 100MPa, and in the compressive zone are slightly smaller than

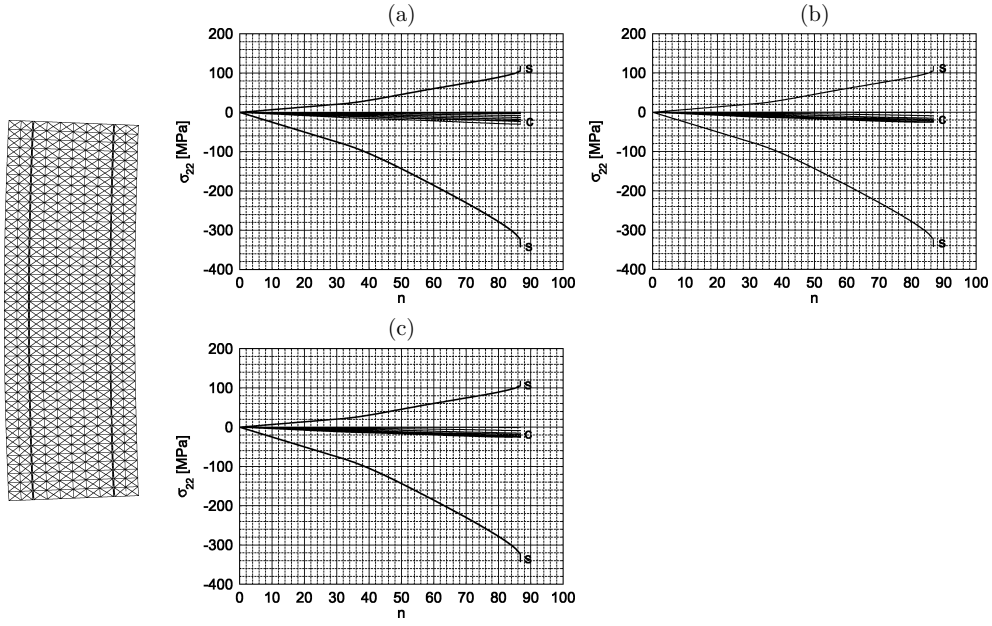

Figure 14. FE-calculations: deformed mesh ($P = 80\text{kN}$) and vertical normal stresses versus load step n at (a) $H = h$, (b) $H = 0.75h$, and (c) $H = 0.5h$ for the case of $h = 0.24\text{m}$, $e/b = 0.3$, $\rho_1 = \rho_2 = 0.99\%$ and hinge-end conditions (s – steel, c – concrete)

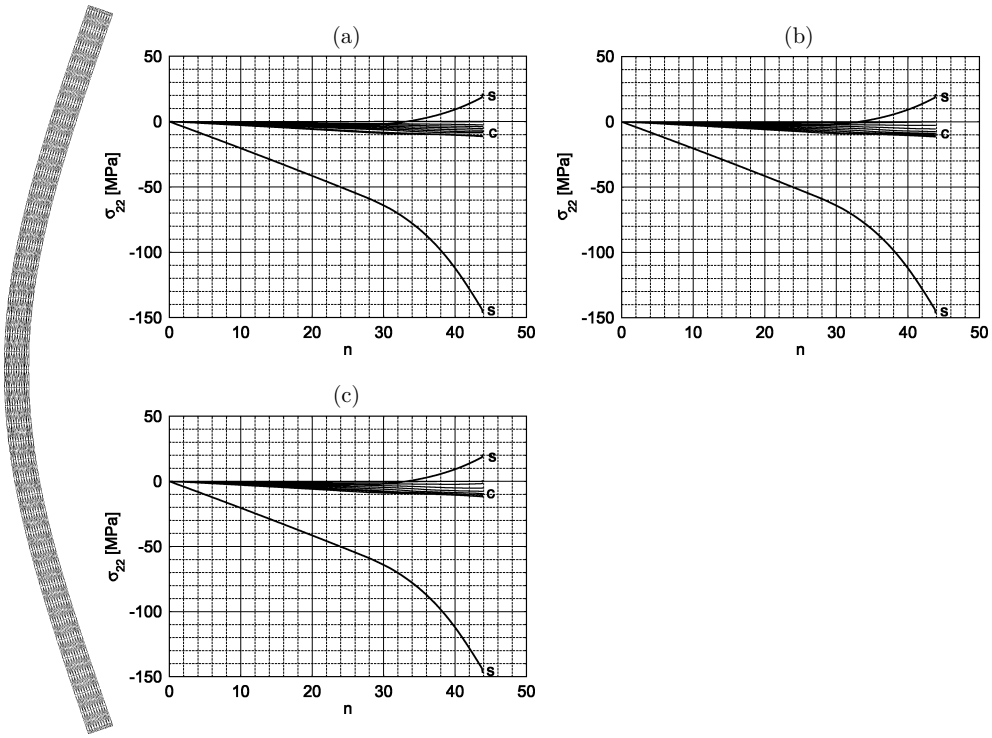

Figure 15. FE-calculations: deformed mesh ($P = 40$kN) and vertical normal stresses versus load step n at (a) $H = h$, (b) $H = 0.75h$ and (c) $H = 0.5h$ for the case of $h = 2.4$m, $e/b = 0.3$, $\rho_1 = \rho_2 = 0.99\%$ and hinge-end conditions (s – steel, c – concrete)

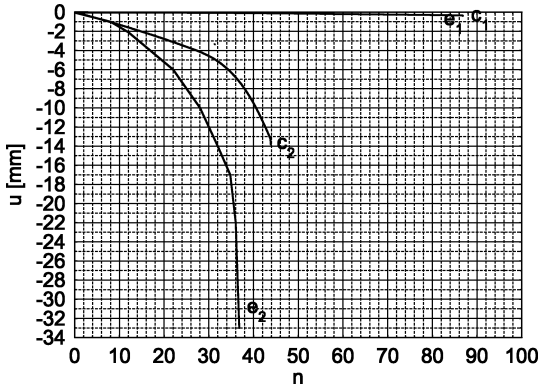

Figure 16. Load-deflection diagrams from experiments and FE-calculations (e – experiment, c – calculation, 1 – short column, 2 – slender column)

$f_{\gamma d}$. For a slender column they are 20MPa and 140MPa, respectively. In both cases, the compressive strength of concrete is obtained.

The ultimate loads from calculations were 87kN (short column) and 44kN (slender column), respectively. These values compare well with experimental ones equal to 83kN and 35–38kN, respectively. In the case of lateral deflections at the mid-height, the numerical results result in 0.45mm (short column) and 15mm (slender

column), and the experimental values are 0.4mm (short column) and 30–33mm (slender column).

The FE-analysis was also performed with $f_{cc} = 1.25 f_c$. In this case, one obtained the ultimate load 90kN with a short column and 62kN with a slender column.

6. Conclusions

The numerical results from the FE-analysis on the behaviour of reinforced concrete elements under eccentric loading are in satisfactory agreement with experimental results. They show that:

The bearing capacity of elements increases with decreasing slenderness, eccentricity, degrees of freedom at both ends, and increasing reinforcement area in the more compressed zone.

A symmetric reinforcement is inefficient because the reinforcement located on the less compressed side never yields.

The vertical normal stresses can change in concrete and reinforcement along the element height.

The FE-studies for reinforced concrete elements under eccentric loading will be continued. In the next step, a more realistic constitutive relation for concrete will be used [1, 2, 27, 40]. A non-local approach [47, 54] will be adopted to obtain a well-posed boundary value problem. The numerical results will be directly compared with experiments.

References

[1] Klisiński M and Mróz Z 1988 *Description of Inelastic Deformation and Degradation of Concrete*, Script, Technical University of Poznan, Poznan, pp. 1–168 (in Polish)

[2] El-Metwally S E and Chen W F 1989 *Comput. Struct. J.* **32** (6) 1203

[3] Klisiński M and Mróz Z 1998 *Int. J. Solids and Structures* **24** 391

[4] Baglin P S and Scott R H 2000 *ACI Struct. J.* **97** (6) 886

[5] Kim J and Yang J 1995 *Engng. Struct.* **17** (1) 39

[6] Makovi J 1969 *Über den Einflußder Hysteresis in the Arbeitslinie des Betons auf das Verformungs- und Tragverhalten exzentrisch belasteter Stahlbetondruckglieder*, PhD Thesis, Darmstadt University

[7] Gruber L and Menn Ch 1978 *Berechnung und Bemessung schlanker Stahlbetonstützen*, Bericht 84, Institut für Baustatik, ETH Zürich

[8] Kiedroń K 1980 *Method for Calculations of Critical Force of Colums Subject to Eccentric Compression*, PhD Thesis, Technical University of Wroclaw (in Polish)

[9] Bilinger M and Symons M 1995 *Proc. CIA/FIP Conf.*, Brisbane, pp. 223–232

[10] Lloyd N A and Rangan B V 1996 *ACI Struct. J.* **93** (6) 631

[11] Szuchnicki W 1973 *Proc. Polish Conf. Civil Engineers, PZITB*, Krynica (in Polish)

[12] Kordina K and Warner R F 1975 *Über den Einflußdes Kriechens auf die Ausbiegung schlanker Stahlbetonstützen*, Deutscher Ausschußfür Stahlbeton, Berlin, Heft 250

[13] Gardner N J, Ramkrishna M G and Tak-Fong W 1992 *ACI Struct. J.* **89** (5)

[14] Oleszkiewicz S, Ruppert J and Najib S 1973 *Proc. Polish Conf. Civil Engineers, PZITB*, Krynica (in Polish)

[15] Korzeniowski P 1997 *Archives of Civil Engineering*, Warsaw **XLIII** (2) 149

[16] Korzeniowski P 2000 *Confined Reinforced-concrete Columns*, Publication of the Gdansk University of Technology, Gdansk, pp. 1–133 (in Polish)

[17] Korzeniowski P 1996 *Analysis of Slender Columns Subject to Eccentric Compression*, PhD Thesis, Gdansk University of Technology (in Polish)

[18] Fragomeni S and Mendis PA 1997 *J. Struct. Engng., ASCE* **123** (5) 680

[19] Mendis P A 2000 *ACI Struct. J.* **97** (6) 895
[20] Liu T C Y, Nilson A H and Slate F O 1977 *J. Engng. Mech. Div. ASCE* **103** 423
[21] Palaniswamy R and Shah S P 1974 *J. Struct. Div. ASCE* **100** 901
[22] Kompfner T A 1983 *Ein Finites Elementmodell für die geometrisch und physikalisch nichtlineare Berechnung von Stahlbetonschalen*, PhD Thesis, Stuttgart University
[23] Stempniewski L 1990 *Flüssigkeitsgefüllte Stahlbetonbehälter unter Erdbebeneinwirkung*, PhD Thesis, Universität Karlsruhe
[24] Mroz Z 1972 *Mathematical Models of Inelastic Concrete Behaviour*, University Waterlo Press, pp. 47–72
[25] Chen A C T and Chen W F 1975 *J. Engng. Mech. Div. ASCE* **101** 465
[26] Willam K J and Warnke E P 1975 *IABSE Seminar on Concrete Structures Subjected to Triaxial Stress*, Bergamo, Italy, pp. 1–31
[27] Pietruszczak S, Jiang J and Mirza F A 1988 *Int. J. Solids Structures* **24** (7) 705
[28] Bazant Z P and Bhat P D 1976 *J. Engng. Mech. Div. ASCE* **102** 701
[29] Bazant Z P and Shieh C L 1978 *Nucl. Engng. Des.* **47** 305
[30] Bazant Z P and Kim S S 1979 *J. Engng. Mech. Div.* **105** 407
[31] Dragon A and Mróz Z 1979 *Int. J. Engng. Sci.* **17** 21
[32] Vervuurt A, van Mier J G M and Schlangen E 1994 *Comp. Methods and Advances in Geomechanics* (Siriwardane and Zaman, Eds.), Balkema, Rotterdam, pp. 713–718
[33] de Borst R 1986 *Non-linear Analysis of Frictional Materials*, PhD Thesis, Delft University
[34] Majewski S 1994 *Proc. Conf. KILiWP*, Krynica, Poland, pp. 129–136 (in Polish)
[35] Bresler B and Pister K S 1958 *ACI Journal* **55** (9) 321
[36] Pramono E 1988 *Numerical Simulation of Distributed and Localised Failure in Concrete*, PhD Thesis, University of Colorado-Boulder
[37] Etse G 1992 *Theoretische und numerische Untersuchung zum Diffusen und Lokalisierten Versagen in Beton*, PhD Thesis, Karlsruhe University
[38] Buyukozturk O 1977 *Computers and Structures* **7** 47
[39] Klisinski M 1985 *Degradation and Plastic Deformation of Concrete*, PhD Thesis, Polish Academy of Sciences (in Polish)
[40] Menetrey P and Willam K J 1995 *ACI Struct. J.* **92** (3) 311
[41] Tejchman J 1997 *Publication Series of the Institut for Rock and Soil Mechanics, University of Karlsruhe* **140** pp. 1–350
[42] Mühlhaus H B 1989 *Ing. Arch.* **59** 124
[43] Tejchman J and Wu W 1993 *Acta Mechanica* **99** 61
[44] de Borst R, Mühlhaus H B, Pamin J and Sluys L Y 1992 *Proc. 3rd Conf. Comp. Plasticity* (Owen D R J, Onate E and Hinton E, Eds.), Pineridge Press, Swansea, pp. 483–508
[45] Tejchman J, Herle I and Wehr J 1999 *Int. J. Num. Anal. Meth. Geomech.* **23** 2045
[46] Bazant Z and Lin F B 1988 *Int. J. Num. Meth. Engng.* **26** 1805
[47] Brinkgreve R 1994 *Geomaterial Models and Numerical Analysis of Softening*, PhD Thesis, University Delft
[48] Sluys L J 1994 *Wave Propagation, Localisation and Dispersion in Softening Solids*, PhD Thesis, University Delft
[49] Loret B and Prevost J H 1991 *J. Engng. Mech. ASCE* **117** 907
[50] Groen A E 1997 *Three-dimensional Elasto-plastic Analysis of Soils*, PhD Thesis, University Delft
[51] Bathe H J 1982 *Finite Element Procedures in Engineering Analysis*, Prentice-Hall, Inc., Englewood Cliffs, New Jersey
[52] Ortiz M and Simo I C 1986 *Int. J. Num. Meth. Engng.* **23** 353
[53] Godycki-Ćwirko T 1982 *Mechanics of Concrete*, Arkady, Warsaw (in Polish)
[54] Akkermann J 2000 *Rotationsverhalten von Stahlbeton-Rahmenecken*, Dissertation, Institut für Massivbau, Universität Karlsruhe